Journal of Materials Chemistry C

Plasma Treatment of ITO Cathode to Fabricate Free Electron Selective Layer In Inverted Polymer Solar Cells

Journal:	*Journal of Materials Chemistry C*
Manuscript ID:	TC-ART-08-2014-001777
Article Type:	Paper
Date Submitted by the Author:	11-Aug-2014

Complete List of Authors:	Zhang, Chunmei; Beijing Institute of Graphic Communication, Qi, Lei; Beijing Institute of Graphic Communication, Chen, Qiang; Beijing Institute of Graphic Communication, Laboratory of Plasma Physics and Materials Lv, Longfeng; Beijing Jiaotong University, Ning, YU; Beijing Jiaotong University, Hu, Yifeng; Beijing Jiaotong University, Hou, Yanbing; Beijing Jiaotong University, Teng, Feng; Beijing Jiaotong University,

Plasma Treatment of ITO Cathode to Fabricate Free Electron Selective Layer In Inverted Polymer Solar Cells

Chunmei Zhang †‡, Lei Qi †, Qiang Chen*†, Longfeng Lv ‡, Yu Ning ‡, Yufeng Hu ‡, Yanbing Hou ‡, and Feng Teng *‡

†Laboratory of Plasma Physics and Materials, Beijing Institute of Graphic Communication, Beijing 102600, China

‡ Institute of Optoelectronic Technology, Beijing Jiaotong University, Beijing 100044, China

Abstract: With Ar plasma treatment of the indium tin oxide (ITO) cathode we achieve an efficient inverted bulk heterojunction solar cells which require no electron selective layer based on poly (3-hexylthiophene):[6,6]-phenyl C_{61} butyric acid methyl ester. The plasma treatment improves the power conversion efficiency of the device from 1.07% to 3.57%, with fill factor of 66 %, open-circuit voltage of 0.60 V, and short-circuits current of 9.03 mA/cm^2. This result is comparable to the regular inverted devices with an additional electron selective layer. The Kelvin probe detects a reduction of ITO work function by ~0.45 eV after plasma treatment, which finally leads to the increase of built-in potential and of faster carrier extraction. As a result, a good device performance is achieved. Since the electron selective layer becomes unnecessary, our strategy suggests a simple way to achieve efficient inverted organic solar cells.

Keywords: free electron-selective layer, inverted bulk heterojunction solar cell, plasma treatment, ITO, the work function

* Electronic addresses: chenqiang@bigc.edu.cn and fteng@bjtu.edu.cn.

1. Introduction

Bulk heterojunction (BHJ) polymer solar cell (PSC) is one of the most promising photovoltaic techniques due to the advantages such as solution processing, low-cost, lightweight and flexibility [1-2]. Recently, inverted PSCs have attracted broad attentions based on the several obvious advantages [3-7]. Opposite to normal structure BHJ PSCs in which indium tin oxide (ITO) is used as an anode to collect holes and a low-work-function metal as cathode to collect electrons, the inverted PSCs use ITO as cathode and the high-work-function metal as anode. Because of avoiding the need to use of the low-work-function metal electrode which oxidizes easily in the environment of air or poly (3,4-ethylenedioxythiophene): poly (styrenesulfonate) hole-transporting layer whose acidity etch underlying ITO over time, inverted PSC devices demonstrate better ambient stability [8]. In addition, inverted configuration demonstrates the merit of the vertical phase separation and concentration gradient in the active layers [9-10]. The high record power conversion efficiency (PCE) of 9.2% achieved by an inverted PSC was reported recently [11].

Because of the low electrical resistivity and high transparency in the visible range, ITO is widely used as an electron-collecting electrode in inverted PSCs. The work function of ITO is about 4.5-4.7 eV, which lies between the typical highest occupied molecular orbital (HOMO) and the lowest unoccupied molecular orbital (LUMO) of common electron acceptor materials [5]. In order to efficiently extract photo-generated electrons in an inverted PSC, different types of electron selective layers with low work function (also known as cathode interlayers, electron transporting layers, or hole blocking layers) are popularly used to modify the surface of ITO, including n-type metal oxides such as zinc oxides and titanium oxides [5-7], self-assembled cross-linked fullerene [8], *n*-type metal carbonates such as cesium carbonate [12], and low-work-function metals such as calcium and magnesium [13], etc. Despite the significantly improved device performance, inserting cathode interlayer actually complicates the fabrication process of PSC device. Plasma treatment, as known, can tune the ITO work function by changing the surface constituents, has been widely used in the area of organic electroluminescent devices [14-16]. It might be also effective in the organic solar cells.

In this work, we demonstrate its fruitful applications in inverted PSCs. With Ar plasma treatment, the inverted BHJ PSC without cathode interlayer based on poly (3-hexylthio- phene):[6,6]-phenyl C61 butyric acid methyl ester (P3HT/PCBM) exhibits a PCE of 3.57%, which is comparable to the regular

inverted PSCs with an additional cathode interlayer. Additionally, during plasma treatment the temperature of the ITO substrate is less than 60ºC, the technology is compatible with the fabrication of devices on flexible substrates by roll-to roll process.

2. Experimental details

2.1 Plasma treatment of ITO

Before plasma treatment the ITO substrates were cleaned in ultrasonic baths by a sequence of detergent solution, acetone, deionized water and ethanol for 30 min respectively, and then dried by nitrogen stream. The cleaned ITO was then noted as the pristine ITO. Afterwards, the ITO substrates were transferred into plasma chamber. When the chamber was evacuated to the base pressure of 2×10^{-4} Pa, Ar gas was flowed into the chamber at the flow rate of 10 sccm. A microwave power (150 W in applied power, 2450 MHz in frequency) was applied to generate plasma in electron cyclotron resonance (ECR) mode. The ITO substrates were treated by Ar plasma for 3 min. Then, the ITO substrates were transferred and stored in the ambient environment for characterization and device fabrication.

2.2 Device fabrication

The inverted PSC based on the plasma treated ITO substrates was fabricated as followings: 1, 2-dicholorobenzene solution composed of P3HT (Rieke Metals, 17 mg/ml) and PCBM (Nano-C, 17 mg/ml) was spin-coated onto the treated ITO at 800 rpm for 25 s in the nitrogen-filled glove box (< 0.1 ppm H_2O and O_2) and then annealed at 110ºC for 10 min. MoO_3 (10 nm in thickness) and Ag (100 nm in thickness) as electrodes were thermally evaporated onto the active layer. The assembled structure of cell is plasma treated ITO/P3HT:PCBM/MoO_3/Ag, and the area of each cell is 4.5 mm^2. As comparison the cell based on the pristine ITO was also assembles in inverted PSC, and the structure is pristine ITO/ P3HT:PCBM/MoO_3/Ag.

2.3 Characterization and measurement

The pristine and plasma treated ITO were characterized by X-ray photoelectron spectroscopy (XPS) using ESCALAB 250 XPS Analysis System with a monochromated Al *Ka* X-ray source for surface chemical composition. Surface roughness and morphology were acquired by atomic force microscopy

(AFM, Veeco Dimension 3100). The work function of ITO was measured with the Kelvin Probe (SKP5050, KP technology Ltd., UK, Au reference) method and the sheet resistance was detected with the four-point probe method. Current density-voltage (J-V) characteristics of the assembled devices were recorded with a Keithley 4200 sourcemeter. An AM 1.5 solar simulator (ABET Technologies) at 100 mW/cm^2 intensity was used to provide illumination. The capacitance-voltage (C-V) measurements were conducted using a Keithley 4200-SCS with an AC bias of 25 mV and the data were recorded at a frequency of 3 kHz. For the transient short-circuit photocurrent measurement, a square-pulsed optical excitation of 200 μs was generated from a 525 nm high-brightness LED driven by a function generator and a 50 Ω input termination of the oscilloscope was used. To test the photo-stability of the device with plasma treated ITO, the device was continuously irradiated with AM 1.5G simulated solar illumination at 100 mW/cm^2 intensity for 80 h in a dry N_2 environment. The measured temperature of the photo-irradiated samples was kept at about 45 °C. The photovoltaic output parameters were measured at fixed interval times during this period.

3. Results and discussion

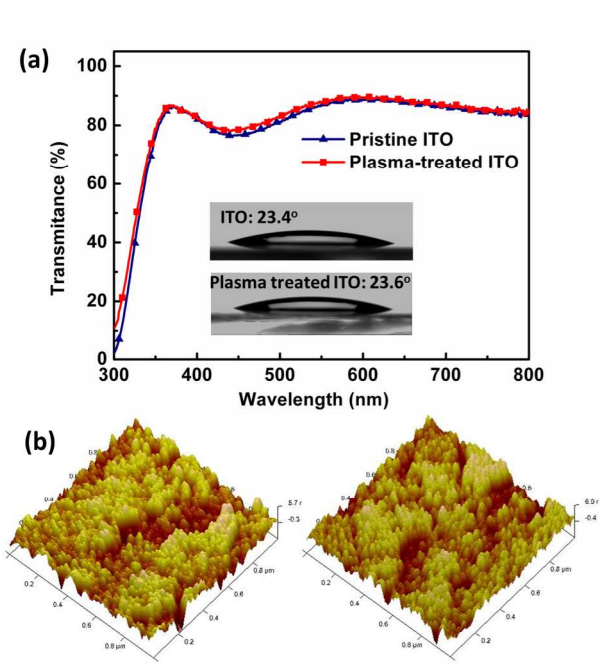

Fig. 1 (a) The transmission spectrum of the pristine and plasma treated ITO glasses (the inset is the water contact angle of both samples); (b) The AFM images of the pristine (left) and the plasma-treated ITO glasses (right). The size is 1x1 μm^2.

The optical transmission spectrum and the AFM images of the pristine and plasma treated ITO are obtained and the results are shown in Fig. 1. The water contact angle measurements of ITO are shown as inset. Comparing to the pristine, AFM images indicate that there are no significant changes in morphology after plasma treatment, and the root-mean-square (RMS) roughness value only increases from 1.35 nm to 1.59 nm. In the visible range the transmittance of ITO substrate is related to the grain-boundary scattering [17]. Since the size of grains in ITO film is not obviously altered in AFM images, the transmittances of the pristine and plasma-treated ITO are identical as Fig. 1 exhibits.

The surface energy of ITO is characterized by the measurement of water contact angle. The negligible variation from 23.4^{o} to 23.6^{o} means that Ar plasma treatment does not graft any polar groups on the surface. We then measured the sheet resistance values of the pristine and plasma treated ITO. The sheet resistance values of ITO are near identical for both samples, varying from 14.2 to 14 Ω/□.

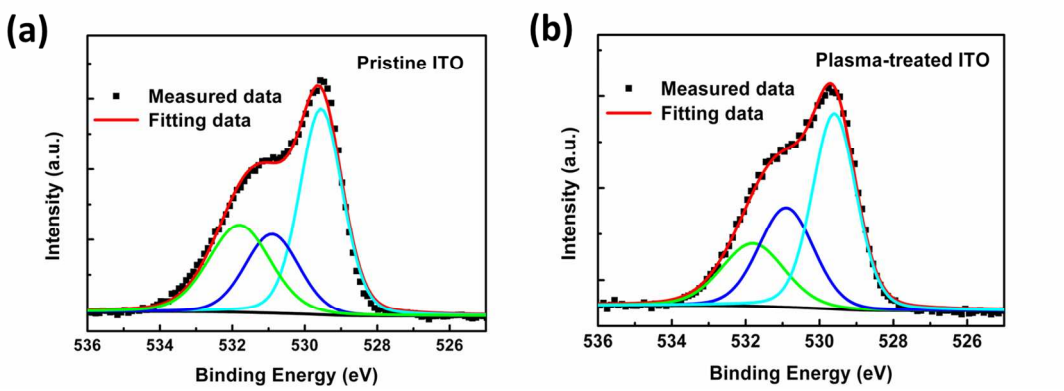

Fig. 2 O1s XPS analysis of (a) the pristine ITO, (b) plasma-treated ITO.

Then, we guess the chemical component after the treatment might be changed. Fig. 2 shows the O1s XPS spectra of the pristine and plasma-treated ITO. The O1s cores are fitted with three components. The peak at 531.9 eV is assigned to the super-imposed peak of the O-H, O-C and O-O bonds absorbed on the ITO surface (O_{III}). The peaks at 531.0 eV (O_{II}) and 529.7 eV (O_{I}) are assigned to the oxygen in oxide lattice with and without oxygen vacancies, respectively [18-19]. The appearance of O_{III} peak indicates the oxygen contamination of the ITO surface, which may be attributed to the exposure of samples to air before the XPS measurement. If the sample is etched by the Ar ion in the XPS chamber and then is measured in-situ, the surface oxygen (O_{III}) and carbon contamination can be removed exactly (Fig. S1, S2).

After Ar plasma treatment, the intensity of O_{II} is relatively higher than that of O_I, and the ratio of O_{II} /O_I increases from 0.47 to 0.61, indicating that plasma treatment increases the concentration of oxygen vacancies in the ITO film. Since oxygen vacancies form donor states, the increase of the oxygen vacancy concentration is expected to cause an upward shift of the Fermi energy of ITO and to decrease the work function [20]. Thus we measured the work function of ITO by Kelvin Probe (KP) method. It is found that a 0.45 eV decrease of the ITO work function is achieved after Ar plasma treatment. We then confirmed the decrease of ITO work function by ultraviolet photoelectron spectroscopy (UPS) measurement, which are shown in Figure S3. The result is consistent with the KP data, a notable reduction (0.53 eV) of the work function after Ar plasma treatment was obtained. The discrepancy between the work function values measured by two approaches: KP and UPS, may be due to the different working mechanisms and measurement environment. In KP method it measures the changes in contact potential difference between the Au reference and the samples, and then to calculate the work function; while in UPS method it is subtracting the energy of the incident beam from the difference between the Fermi edge and the low-energy cut-off of secondary electrons to obtain the work function. Besides, KP is performed in ambient atmosphere and the absorbed molecular or atomic species can induce the absolute work function shift, UPS spectra are carried out in ultra-high vacuum, where the high energetic photons irradiation (He I line) will cause other effects, e.g. desorbing molecular or atomic species from surface [21]. Nevertheless, both measurements confirm the decreasing trend of work function after Ar plasma treatment. We then use the 0.45 eV as the decrease of the ITO work function in following analysis because the measurement environment of KP is closer to the experimental conditions used for fabrication of cells.

The J-V characteristics of the inverted devices with pristine and plasma treated ITO cathodes are shown in Fig. 3. Under illumination, the J-V curve of the device with the pristine ITO rises quickly around V = 0 V and *S*-shaped characteristic appears in the fourth quadrant, which leads to a small open-circuit voltage (V_{oc}) of 0.33 V and a comparatively low FF of 40% (Fig. 3(a)). Although the short circuit current is as high as 8.23 mA/cm^2, the PCE value is still only 1.07%.

For the device with plasma treated ITO cathode, the J-V curve exhibits normal exponential diode-like characteristics. The *S*-shaped characteristic in the fourth quadrant disappears, resulting in the increase of PCE value from 1.07% to 3.57%, with fill factor of 66%, open-circuit voltage of 0.60 V, and

short-circuits current of 9.03 mA/cm^2. Table 1 lists the derived performance parameters from Fig. 3 (a) and the averaged data with standard deviation of five batches of identically processed solar cells, each batch includes four individual cells. One can see that the performance of the cells in the same batch varies slightly from cell to cell (Fig. S4).

In the absence of cathode interlayer, the inverted solar cell with plasma treated ITO cathode now demonstrates the pretty performance compared to the regular inverted solar cells with additional cathode interlayer [22]. Since the ITO cathode exhibited almost the same surface energy and surface morphology before and after plasma treatment, the vertical phase separation and the morphology of photoactive layers should be similar in the two types of devices [9]. Then we believe that the improvement of the PCE should be attributed to the decrease of the ITO work function.

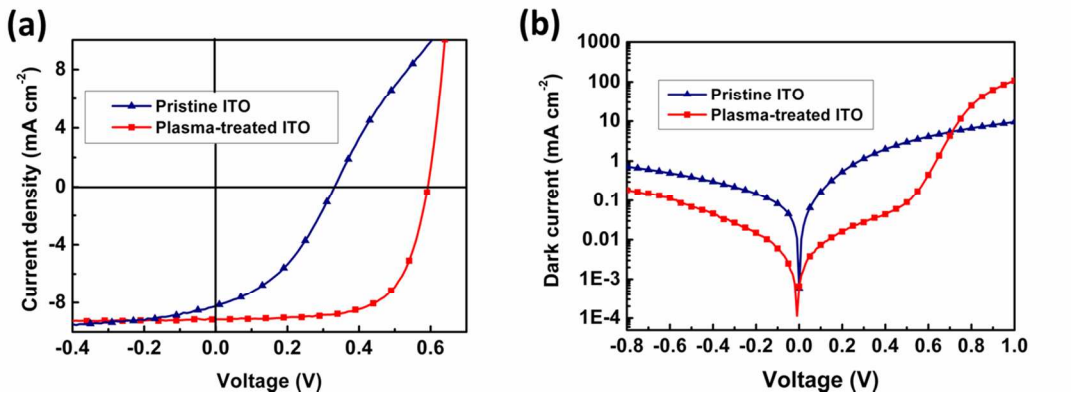

Fig. 3 The characteristics of J-V versus voltage in inverted solar cells for pristine and plasma treated ITO cathodes, (a) under illumination; (b) in dark.

Table 1. The derived solar cell performance parameters from Fig. 3, including the average and standard deviation (s.d.) values of five batches of identically processed solar cells

Cathode of the device	V_{OC} (V)	J_{SC} (mA/cm^2)	FF	PCE (%)
Pristine ITO (average ± s.d.)	0.32 ± 0.03	8.09 ± 0.20	0.38 ± 0.04	0.98 ± 0.18
Plasma-treated ITO (average ± s.d.)	0.60 ± 0.01	8.98 ± 0.18	0.65 ± 0.02	3.51 ± 0.07

The J-V characteristics of the devices in dark condition are presented in Fig. 3(b). It can be clearly seen that the device with plasma treated ITO exhibits a larger turn-on voltage (~ 0.5 V), while that for the pristine ITO assembled cell exhibits injection currents with virtually no turn-on voltage. This implies that the built-in potential (V_{bi}) across the device, which is responsible for exciton dissociation and the

upper limit for the attainable V_{oc}, is increased upon the plasma treated ITO [23, 24]. In addition, comparing with the pristine ITO assembled device, the device with plasma treated ITO shows a brilliant diode quality with a lower leakage current and a higher rectification ratio. This proves that the plasma treated ITO creates a high conductive path for electron extraction, which can explain the enhanced FF of the device [23].

Fig. 4(a) compares the capacitance-voltage (C-V) characteristics of devices with pristine and plasma treated ITO. The measurements were carried out in the dark condition at the room temperature. The C-V curves in devices based on organic semiconductors are usually used to derive the Mott-Schottky characteristics and even to provide the flat-band voltage (V_{fb}) (equivalent the built-in potential, V_{bi}) [23-26]. The Mott-Schottky characteristics for both samples are shown in Fig. 4(b), where $C^{-2} = 2(V_{fb} - V)/(A^2 q\varepsilon\varepsilon_0 N_A)$, V is the applied voltage, A corresponds to the device active surface (4.5 mm^2), q accounts for the elementary charge, ε is the relative dielectric constant of the semiconductors (assumed to be 3), ε_0 is the permittivity of the vacuum, and N_A is the organic semiconductors doping density. Then the V_{fb} (V_{bi}) could be obtained through the intersecting on voltage axis by the simulated tangent line from the curve. For the pristine ITO based devices, the V_{bi} is 0.08 V; while for plasma treated ITO based device, the V_{bi} increases to 0.41 V. The increase in V_{bi} matches the increase in V_{oc} and indicates that the plasma treated ITO indeed attributes an increase of the device built-in field.

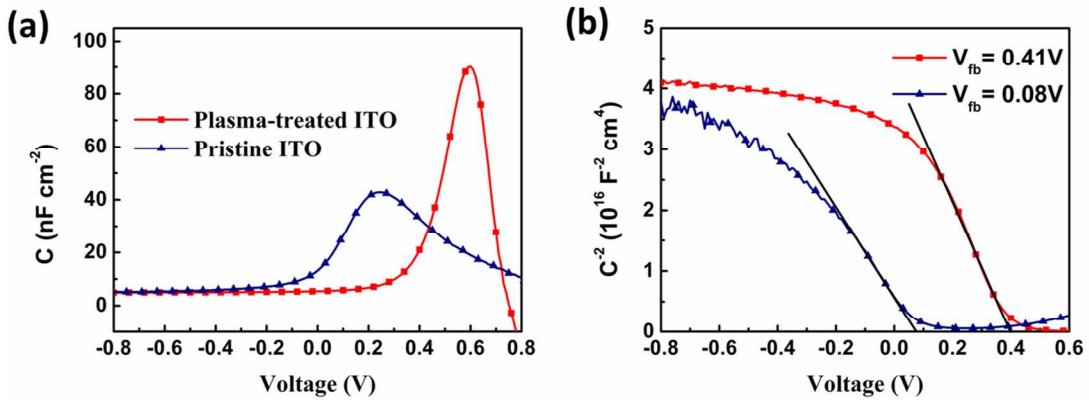

Fig. 4 (a) Comparison of C-V response of inverted solar cells with pristine and plasma treated ITO cathodes. (b) Mott-Schottky characteristics of the devices exhibiting a linear relationship (straight lines) at low forward bias. The flat-band potential V_{fb} in the inset is indicated for each curve.

The enhanced internal electric field was future evident by the short-circuit current measurement. Fig. 5 presents the short-circuit current response of the two devices to 200 μs square-pulse optical

excitation from a 525 nm high-brightness LED driven by a function generator. The device with pristine ITO cathodes exhibits slow turn-on and turn-off dynamics, with very little change in the shape of transient photocurrent curves under different intensities of excitation light (Fig. 5(a) and (b)). The rise/fall times of the device (defined as the time taken to go from 10% to 90% of the full response) are about 14 μs and are independent of light intensity. For the device with plasma treated ITO cathode (Fig. 5(c) and (d)), on the other hand, the photocurrent dynamics become systematically faster. The rise/fall times of the device are about 7 μs and are also independent of light intensity. Considering the previous transient photocurrent studies on P3HT/PCBM devices, the light-intensity independence of the photocurrent rise/fall time reveals trap-free charge transport in the device [27]. In the device with plasma treated ITO cathode, the faster short-circuit photocurrent response at turn-on and turn-off suggests a faster transport of charge occurrence, which is mainly caused by the higher internal electric field [27].

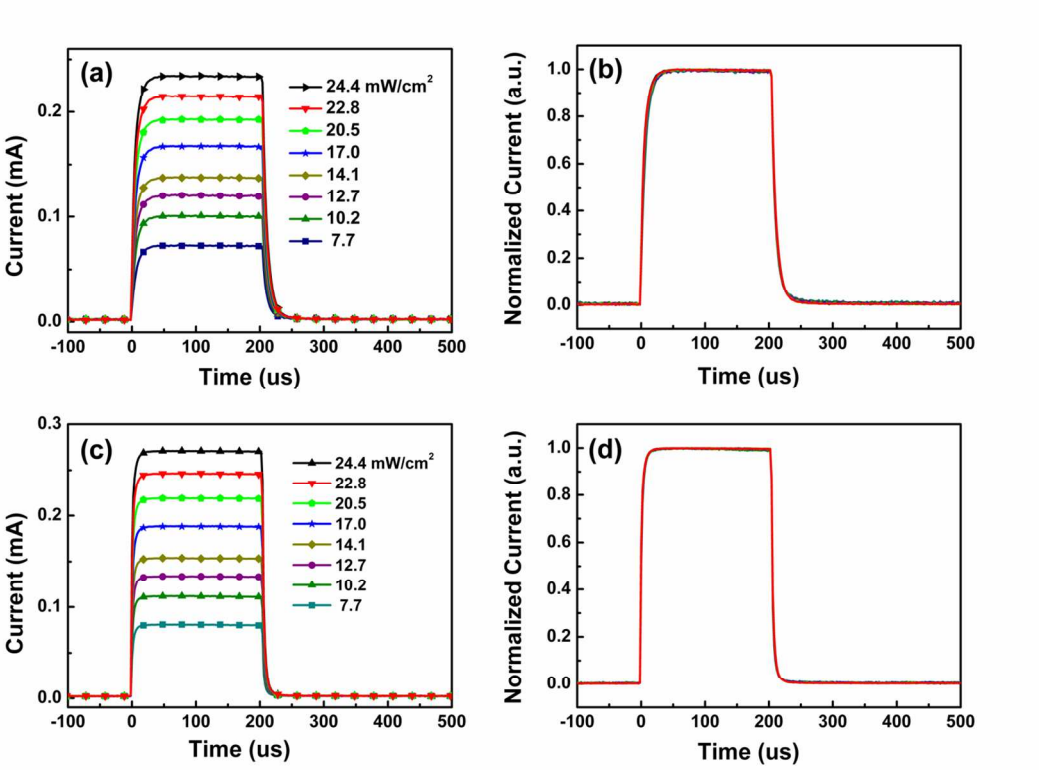

Fig. 5 The transient short-circuit photocurrent of the device in response to a 200 μs square pulse with wavelength in 525 nm for various intensities. a, b—with pristine cathode; c, d—with Ar plasma treated ITO cathode; (a), (c) are un-normalized traces; and (b), (d) are normalized traces.

On the basis of results discussed above, we try to propose a physical model to explain the favorable role of plasma treated ITO cathode. For the inverted PSC, the direction of the built-in potential

V_{bi} is from ITO cathode to anode, which is beneficial for the electrons drifting towards ITO cathode and holes drifting towards Ag anode [28]. The decrease of the cathode work function can increase the built-in potential and then enhance the extraction efficiency of photo-generated carriers [26]. In our work, the built-in potential of the device increase from 0.08 V to 0.41 V after the plasma treatment. As a result, the good device performance and the faster turn-on and turn-off transient photocurrent response are achieved. In addition, for the devices with pristine ITO cathode, the large energetic mismatch between the work function of ITO substrate (*Wc*, 4.7 eV) and the energy of the negative integer transfer state (E_{ICT-}) of PCBM (4.3 eV) leads to the barriers for charge injection, which induces the *S*-shaped J-V curve in the fourth quadrant [28-30]. When the *Wc* is varied from 4.7 eV to 4.25 eV after plasma treatment, E_{ICT-} of PCBM now is only a little bit higher than *Wc*, which result in a desirable Ohmic contact between ITO and PCBM and consequently reducing the electron accumulation at ITO cathode.

Furthermore, we studied the aging of plasma treated ITO on the cell efficiency by storing them in air under ambient condition for different times, and then fabricating the inverted devices with these treated ITO substrates. The J-V curves of the assembled cells are shown in Fig. 6(a), and the parameters of photovoltaic performance are summarized in Table 2. After the ITO was stored for 40 days the PCEs of devices decreased slightly from 3.57% to 3.47%, and the V_{oc} and FF remained unchanged. This is evident that the shift of the ITO work function after plasma treatment is non-reversible process, and the treated sample has a good stability in air. Wang et al. and Zhou et al. [31-32] have once reported a process to decrease the ITO work function by prolonging UV or solar simulator illumination in nitrogen-filled glove box. However, the reversible behavior after exposed in air again made this method impractical in commercial applications.

Besides the aging of the treated ITO, we examined the stability of the inverted PSCs with Ar plasma treated ITO cathode. It is worth noting that the plasma treated ITO cathode was stored in air for 2 hours before assembled. Un-encapsulated devices were periodically tested during storage in a N_2-filled glove box. As can be seen in Fig. 6 (b), after 60 days of storage in N_2, the PCE of the device was only slightly lower than its original value. We then conclude that inverted PCEs with plasma treated ITO is also much stable.

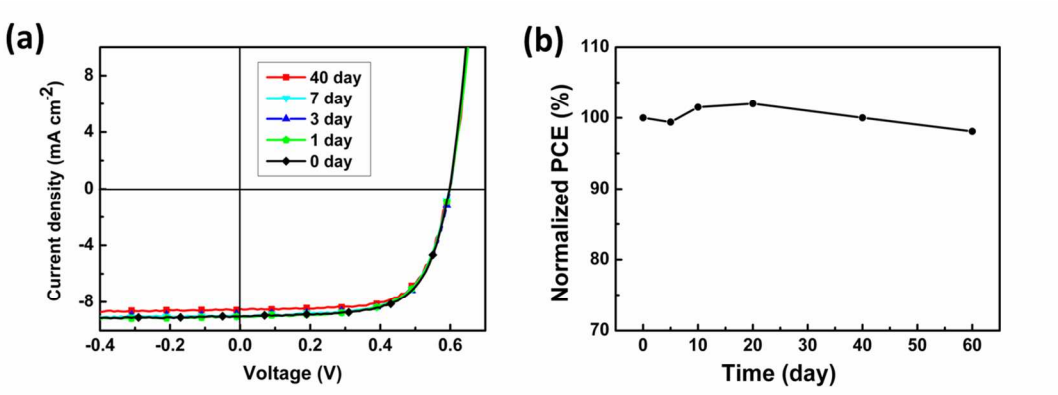

Fig. 6 (a) J-V characteristics of inverted solar cells (under illumination) with aged plasma treated ITO cathodes. (b) The stability of inverted PSCs with Ar plasma treated ITO in N_2-filled glove box. The PCE is normalized to its initial value.

Table 2 The derived solar cell performance parameters from Fig. 6(a), i.e. the plasma-treated ITO substrates were stored in air under ambient conditions for over 40 days before they were used to assemble inverted PSCs.

ITO storage time	V_{OC} (V)	J_{SC} (mA/cm^2)	*FF* (%)	*PCE* (%)
2 hour	0.60	9.03	66	3.57
1 day	0.60	8.99	65	3.51
3 days	0.60	8.83	67	3.56
7 days	0.60	8.98	65	3.51
40 days	0.60	8.50	68	3.47

We explore the photo-stability in the inverted PSCs of free electron selective layer. As known [33, 34] the interface between the ITO and the active layer plays a critical role in the photo-degradation behavior of the devices. In recent years, many studies were focused on the organic/electrode contacts and their influence on device photo-stability behavior [33-35]. We intend to explore the photo-stability of inverted devices with plasma treated ITO. For comparison, we prepared the inverted device with ZnO-modified ITO as the electron selective layer, which is widely used in the inverted devices [36-37]. The structure of the device is ITO/ZnO/P3HT:PCBM/MoO_3/Ag. The experimental detail of the device with ZnO interlayer was shown in supporting information, and the initial efficiency of the device with ZnO layer is 3.21%.

Fig. 7 shows the evolution of normalized cell performance and the alteration of J-V characteristics of the devices under the continuous illumination for both samples. For the device with ZnO interlayer, the light stress causes a 20% loss in V_{OC}, a 28% loss in J_{SC} and a 10% loss in FF after 80 h of continuous light exposure. For the device with plasma-treated ITO, light stress causes a 23% loss in V_{OC}, a 29% loss

in J_{SC} and a 22% loss in FF. Although the losses in V_{OC} and J_{SC} in both devices are similar, the device with plasma treated ITO suffers a more strong loss in FF. As a result, PCE of the devices without interlayer and with ZnO interlayer were decreased by ca. 52% and ca. 43%, respectively. The larger drop of FF in the device with plasma treated ITO might be due to the direct contact between the active layer and the ITO electrode because in the dark condition the performance of device with plasma-treated ITO was degraded very little. So we guess the interaction between the ITO and active layer might occur due to the light exposure period. The active layer-electrode interface causes a little bit less of photo-stable than that in the organic-ITO interface with ZnO interlayer. The photo-degradation mechanism at the active layer-electrode interface will be studied in the future work.

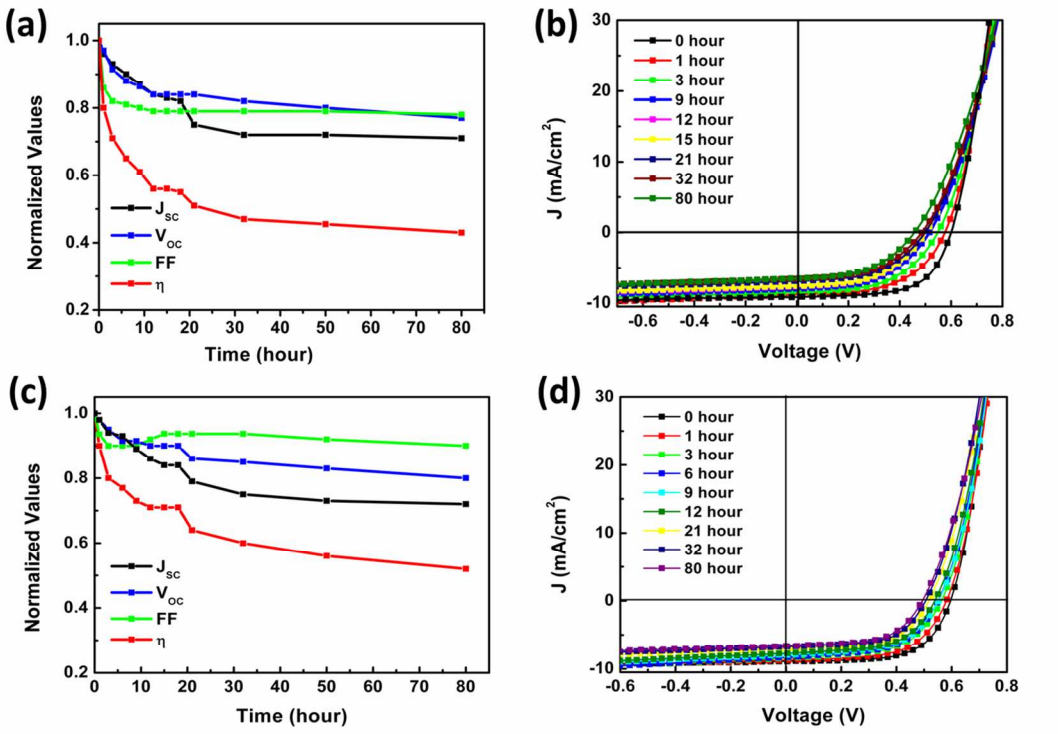

Fig. 7 The evolution of normalized cell performance of the device (a) with plasma-treated ITO and (c) with ZnO layer; the alteration of J-V characteristics of the device with (b) plasma-treated ITO and (d) ZnO layer. All devices were continuously irradiated with AM 1.5G simulated solar illumination at 100 mW/cm^2 intensity in a dry N_2 environment.

4. Conclusions

To summarize, an efficient inverted P3HT/PCBM solar cell without cathode interlayer has been achieved by using Ar plasma treated ITO cathodes. The obtained PCE of 3.57% is comparable to the

regular inverted solar cells based on P3HT/PCBM with additional cathode interlayers. The XPS results reveal that the plasma treatment increases the concentration of oxygen vacancies in the ITO film, which leads to the reduction in the ITO work function. We notice that the work function of plasma treated ITO is remarkably stable. Compared to the device with non-treated ITO cathode, we believe the improved performance is attributed to the increase of built-in potential across active layer and the better energy match between ITO work function and E_{ICT-} of PCBM. Since inserting cathode interlayer becomes unnecessary, our strategy suggests a simple method to achieve cost-effective inverted organic solar cells fabrication.

Acknowledgment

This work was financially supported by the National Science Foundation for Distinguished Yong Scholars of China (61125505), National Natural Science Foundation of China (Grant Nos. 61377028, 11175024, 11375031) and 2011BAD24B01.

References

[1] G. Li, V. Shrotriya, J. Huang, Y. Yao, T. Moriarty, K. Emery, Y. Yang, High-efficiency solution processable polymer photovoltaic cells by self-organization of polymer blends, Nat. Mater. 4 (2005) 864-868.

[2] B. C. Thompson, J. M. J. Frechét, Polymer-fullerene composite solar cells, Angew. Chem. Int. Ed. 47 (2007) 58-77.

[3] M. Glatthaar, M. Miggemann, B. Zimmermann, P. Lewer, M. Riede, A. Hinsch, J. Luther, Organic solar cells using inverted layer sequence, Thin Solid Film. 491 (2005) 298-300.

[4] G. Li, C. W. Chu, V. Shrotriya, J. Huang, Y. Yang, Efficient inverted polymer solar cells, Appl. Phys. Lett. 88 (2006) 253503.

[5] S. Chen, J. Manders, S. Tsang, F. So, Metal oxides for interface engineering in polymer solar cells. J. Mater. Chem. 22 (2012) 24202-24212.

[6] Y. Sun, J. H. Seo, C. J. Takacs, J. Seifter, A. J. Heeger, Inverted polymer solar cells integrated with a low-temperature-annealed sol-gel-derived ZnO film as an electron transport layer, Adv. Mater. 23 (2011) 1679-1683.

[7] C. E. Small, S. Chen, J. Subbian, C. M. Amb, A. W. Tsang, T. H. Lai, J. R. Reynolds, F. So, High-efficiency inverted dithienogermole-thienopyrrolodione-based polymer solar cells, Nature. Photon. 6 (2012) 115-120.

[8] C. H. Hsieh, Y. J. Cheng, P. J. Li, C. H. Chen, M. Dubosc, R. M. Liang, C. H. Hsu, High efficient and stable inverted polymer solar cells integrated with a cross-linked fullerene material as an interlayer, J. Am. Chem. Soc. 132 (2010) 4887-4893.

[9] Z. Xu, L. M. Chen, G. Yang, C. H. Huang, J. Hou, Y. Wu, G. Li, C. S. Hsu, Y. Yang, Vertical phase separation in poly(3-hexylthiophene): fullerene derivative blends and its advantage for inverted structure solar cells, Adv. Funct. Mater. 19 (2009) 1227-1234.

[10] M. C. Quiles, T. Ferenczi, T. Agostinelli, P. G. Etchegoin, Y. Kim, T. D. Anthopoulos, P. N. Stavrinou, D. D. C. Bradley, J. Nelson, Morphology evolution via self-organization and lateral and vertical diffusion in polymer:fullerene solar cell blends, Nature. Mater. 7 (2008) 158-164.

[11] Z. He, C. Zhong, S. Su, M. Xu, H. Wu, Y. Cao, Enhanced power-conversion efficiency in polymer solar cells using an inverted device structure, Nature. Photon. 6 (2012) 591-595.

[12] H. Liao, L. Chen, Z. Xu, G. Li, and Y. Yang, Highly efficient inverted polymer solar cell by low temperature annealing of Cs_2CO_3 interlayer, Appl. Phys. Lett. 92 (2008) 173303.

[13] C. Y. Jiang, X. W. Sun, D. W. Zhao, A. K. K. Kyaw, Y. N. Li, Low work function metal modified ITO as cathode for inverted polymer solar cells, Sol. Energy Mater. Sol. Cells. 94 (2010) 1618-1621.

[14] J. S. Kim, M .Granstrom, R. H. Friend, N. Johansson, W. R. Salaneck, R. Daik, W. J. Feast, F. Cacialli, Indium-tin oxide treatments for single- and double-layer polymeric light-emitting diodes: The relation between the anode physical, chemical, and morphological properties and the device performance, J. Appl. Phys. 84 (1998) 6859.

[15] M. G. Mason, L. S. Hung, C. W. Tang, S. T. Lee, K. W. Wong, M. Wang, Characterization of treated indium-tin-oxide surfaces used in electroluminescent devices, J. Appl. Phys. 86 (1999) 1688.

[16] P. Vacca, M. Petrosino, A. Guerra, R. Chierchia, C. Minarini, D. D. Sala, A. Rubino, The relation between the electrical, chemical, and morphological properties of indium-tin oxide layers and double-layer light-emitting diode performance, J. Phys. Chem. C. 111 (2007) 17404-17408.

[17] W. F. Wu, B. S. Chiou, Effect of annealing on electrical and optical properties of RF magnetron sputtered indium tin oxide films, Appl. Surf. Sci. 68 (1993) 497-504.

[18] J. Kim, D. Lee, J. Kim, S. Yang, J. Lee, Effects of H_2/O_2 mixed gas plasma treatment on electrical and optical property of indium tin oxide, Applied Surface Science. 265 (2013) 145-148.

[19] K. Purvis, G. Lu, J. Schwartz, S. Bernasek, Surface characterization and modification of Indium Tin Oxide in ultrahigh vacuum, J. Am. Chem. Soc. 122 (2000) 1808-1809.

[20] K. Sugiyama, H. Ishii, Y. Ouchi, K. Seki, Dependence of indium-tin-oxide work function on surface cleaning method as studied by ultraviolet and x-ray photoemission spectroscopies, J. Appl. Phys. 87 (2000) 295.

[21] J. Kim, B. Lagel, E. Moons, N. Johansson, I. Baikie, W. Salaneck, R. Friend, F. Cacialli. Kelvin probe and ultraviolet photoemission measurements of indium tin oxide work function: a comparison. Synthetic Metals. 111-112 (2000) 311-314.

[22] L. M. Chen, Z. Xu, Z. Hong, Y. Yang, Interface investigation and engineering-achieving high performance polymer photovoltaic devices, J. Mater. Chem. 20 (2010) 2575-2598.

[23] M. Vasilopoulou, A. Soultati, D. G. Georgiadou, T. Stergiopoulos, L. C. Palilis, S. Kennou, N. A. Stathopoulos, D. Davazoglou, P, Argitis, Hydrogenated under-stoichiometric tungsten oxide anode interlayers for efficient and stable organic photovoltaics, J. Mater. Chem. A. 2 (2014) 1738-1749.

[24] H. Zhou, Y. Zhang, J. Seifter, S. Collins, C. Luo, C. Bazan, T. Nguyen, A. J. Heeger, High-efficiency polymer solar cells enhanced by solvent treatment, Adv. Mater. 25 (2013) 1646-1652.

[25] P. Boix, J. Ajuria, I. Etxebarria, R. Pacios, G. Garcia-Belmonte, J. Bisquert, Role of ZnO electron-selective layers in regular and inverted bulk heterojunction solar cells, J. Phys. Chem, Lett. 2 (2011) 407-411.

[26] J. Chang, Z. M. Kam, Z. Lin, C. Zhu, J. Zhang, J. Wu, TiO_x/Al bilayer as cathode buffer layer for inverted organic solar cell, Appl. Phys. Lett. 103 (2013) 173303.

[27] Z. Li, F. Gao, N. C. Greenham, C. R. McNeill, Comparison of the operation of polymer/fullerene, polymer/polymer, and polymer/nanocrystal solar cells: a transiente photocurrent and photovoltage study, Adv. Funct. Mater. 21 (2011) 1419-1431.

[28] A. Kumar, S. Sista, Y. Yang, Dipole induced anomalous S-shape I-V curves in polymer solar cells, J. Appl. Phys. 105 (2009) 094512.

[29] S. Braun, W. R. Salaneck, M. Fahlman, Energy-level alignment at organic/metal and roganic/organic interfaces, Adv. Mater. 21 (2009) 1450-1472.

[30] W. Tress, S. Corvers, K. Leo, M. Riede, Investigation of driving forces for charge extraction in organic solar cells: transient photocurrent measurements on solar cells showing S-shaped current-voltage characteristics, Adv. Energy Mater. 3 (2013) 873-880.

[31] Y. Zhou, J. W. Shim, C. Fuentes-Hernandez, A. Sharma, K. A. Knauer, A. J. Giordano, S. R. Marder, and B. Kippelen, Direct correlation between work function of indium-tin-oxide electrodes and solar cell performance influenced by ultraviolet irradiation and air exposure, Phys. Chem. Chem. Phys. 14 (2012) 12014-12021.

[32] J. Wang, C. Lu, J. Hsu, M. Lee, Y. Hong, T. Pergn, S. Horng, and H. Meng, Efficient inverted orgainc solar cells without an electron selective layer, J. Mater. Chem. 21 (2011) 5723-5728.

[33] G. Williams, H. Aziz, The effect of charge extraction layers on the photo-stability of vacuum-deposited versus solution-coated organic solar cells, Organic Electronics. 15 (2014) 47-56.

[34] G. Williams, Q. Wang, H. Aziz, The photo-stability of polymer solar cells: contact photo-degradation and the benefits of interfacial layers, Adv. Funct. Mater. 23 (2013) 2239-2247.

[35] M. Lo, T. Ng, H. Mo, C. Lee, Direct threat of a UV-Ozone treated indium-tin-oxide substrate to the stabilities of common organic semiconductors, Adv. Funct. Mater. 13 (2013) 1718-1723.

[36] Z. Liang, Q. Zhang, O. Wiranwetchayan, J. Xi, Z. Yang, K. Park, C. Li, G. Cao, Effects of the morphology of ZnO buffer layer on the photovoltaic performance of inverted polymer solar cells, Adv. Funt. Mater. 22 (2012) 2194-2201.

[37] A. Kyaw, X. Sun, C. Jiang, G. Lo, D. Zhao, D. Kwong, An inverted organic solar cell employing a sol-gel derived ZnO electron selective layer and thermal evaporated hole selective layer, Appl. Phys. Lett. 93 (2008) 221107.

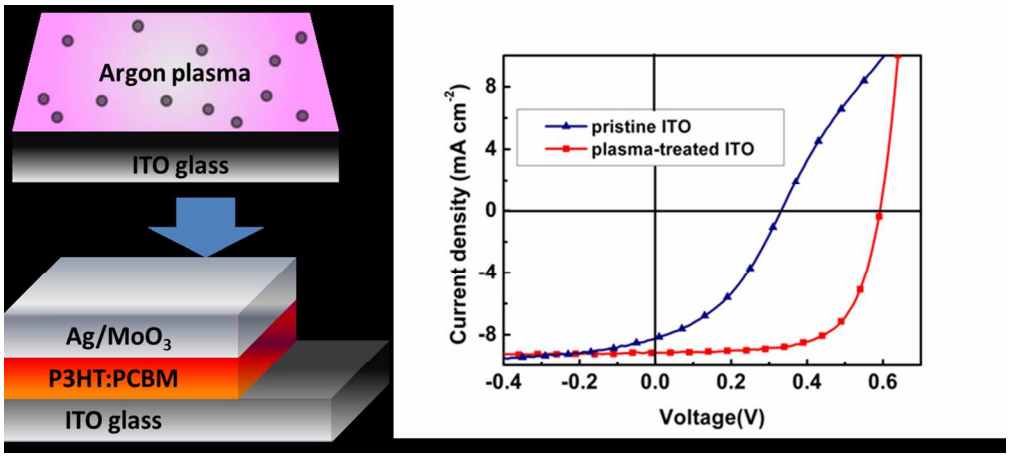

238x106mm (150 x 150 DPI)